

Unmonitored and monitored recurrence in single-photon quantum walks

Xiao-Xiao Chen^{✉,*}, Ya-Jing Wang^{*}, An-Ning Zhang^{✉,†}, Zhe Meng, Qing-Yuan Wu, and Xin-Bing Song[‡]

Center for Quantum Technology Research and Key Laboratory of Advanced Optoelectronic Quantum Architecture and Measurements (MOE),
School of Physics, Beijing Institute of Technology, Haidian District, Beijing 100081, China

Xue-Shun Shi[§]

The 41st Research Institute of CETC, Qingdao 266555, China



(Received 8 March 2024; revised 20 May 2024; accepted 27 June 2024; published 15 July 2024)

Recurrence is an interesting property that describes whether the walker will eventually return to the origin on infinite lattices in classical random walks. Since measurement collapse affects the wave function of the walker, in the quantum case, there are two schemes for studying recurrence properties in quantum walks (QWs) depending on how the measurement process is described. One involves restarting after measurements, known as unmonitored measurements, while the other entails monitoring after each step, referred to as monitored measurements. In this paper, we utilize the dependence of recurrence probabilities on the coin parameter to construct biased-coin QWs on a line and investigate the recurrence properties of both schemes. Based on the bulk-optics framework and using a single-photon source, we experimentally demonstrate the distinct recurrence behaviors resulting from the different evolution processes of the walker in the two schemes. This work showcases diverse recurrence properties in single-particle QW systems, thereby enhancing our understanding of measurement-induced recurrence.

DOI: [10.1103/PhysRevA.110.012219](https://doi.org/10.1103/PhysRevA.110.012219)

I. INTRODUCTION

Classical random walks, or random walks (RWs) for short, are a widely studied stochastic process [1]. An intriguing question regarding RWs is whether the particle eventually returns to the origin. In 1921, Pólya [2] first discussed this question in the context of RWs on infinite lattices and provided a definition of the recurrence probability (also known as the Pólya number), which characterizes the recurrence of RWs. Pólya pointed out the recurrence properties of unbiased RWs as being solely related to the dimensionality of the walk. In one and two dimensions the walk is recurrent (Pólya number equals 1), indicating that the particle will inevitably return to its origin. However, in three and higher dimensions the walk is transient (Pólya number less than 1), and a certain probability that the particle will return to its origin exists [3]. The mathematical proverb “a drunk man will find his way home, but a drunk bird may be lost forever” vividly describes this intriguing phenomenon.

Quantum walks (QWs) were initially proposed by Aharonov *et al.* [4]. They have been extensively studied in various theoretical fields and have also been experimentally demonstrated in a range of physical systems, including trapped atoms [5], trapped ions [6], nuclear magnetic resonance [7], and photonic systems [8–11]. As the quantum

counterpart of RWs, several properties of QWs have been investigated, such as the first detected return [12–17] and the recurrence behavior [18–23]. Štefaňák *et al.* [18] extended the definition characterizing recurrence properties of RWs to the quantum domain and provided an alternative definition for the recurrence probability. In contrast to RWs, the recurrence behavior and the actual value of the Pólya number for QWs depend on the topology of the walk, the choice of the coin operator, and the initial coin state [19]. Since measurement collapse affects the wave function of the system, studying the recurrence of QWs requires a detailed description of the measurement process. The above two definitions correspond to two different schemes for detecting recurrence in QWs. One corresponds to the definition by Štefaňák *et al.*, in which the measurements is performed only once after t steps, without any monitoring in between, and then a new walk starts. This scheme is referred to as the unmonitored-measurement (UMM) scheme [18]. The other scheme, similar to the Pólya definition, requires continuous monitoring of the walker at the origin after the first step and is called the monitored-measurement (MM) scheme [21]. In the classical scenario, the two definitions are considered equivalent in that the recurrence of one definition implies the recurrence of the other and vice versa. This stems from the fact that the recurrence behaviors of both definitions are determined by the asymptote of the probability that the walker returns to the origin after t steps. However, this equivalence no longer holds in the measurements-induced QWs [24,25] as the walker undergoes different evolution processes due to the effect of measurements on the wave function.

*These authors contributed equally to this work.

†Contact author: anningzhang@bit.edu.cn

‡Contact author: songxinbing@bit.edu.cn

§Contact author: shixueshun@ei41.com

Note that a specific example has been examined both theoretically [18,21] and experimentally [22] to show the two schemes are not inequivalent for QWs; e.g., the unbiased QWs on a line exhibit recurrence in the UMM scheme while being transient in the MM scheme. However, most previous studies focused on unbiased walks involving balanced coins and step lengths. There are theories discussing the effects of biased coins and unequal step lengths on the recurrence according to Štefaňák *et al.*'s definition, as well as the implications of the coin parameter and initial coin state for Pólya's definition. Nevertheless, no study has yet investigated and demonstrated the effects of the coin parameter and initial coin state on the recurrence probabilities of both definitions simultaneously. Therefore, it is essential to consider the implications of the coin parameter and initial coin state in both schemes when detecting recurrence in experiments.

In this paper, we simultaneously analyze the coin parameter's impact on the recurrence of the two schemes and demonstrate the disparity in their recurrence probabilities within a biased-coin QW using a single-photon source based on a bulk-optics framework. We conduct a numerical investigation into the recurrence probabilities with varying coin parameters and initial coin states, revealing that the differences in recurrence probabilities between the two definitions are solely determined by the coin parameter. Specifically, we select a biased-coin parameter capable of illustrating significant differences in recurrence probabilities within just a few steps. Consequently, we utilize this specialized coin to perform an experimental demonstration, clearly showcasing distinct recurrence behaviors between UMM and MM schemes resulting from the nature of quantum measurements.

II. RESULTS

Let us consider the coined QWs on a line starting from the origin, with the Hilbert space being a tensor product of the position space $\mathcal{H}_p = \{|x\rangle, x \in \mathbb{Z}\}$ and the coin space $\mathcal{H}_c = \{|\uparrow\rangle, |\downarrow\rangle\}$. Each step of the QW is given by the evolution operator

$$U = S(I \otimes C), \quad (1)$$

where I denotes the unit operator acting on the position space. The shift operator S represents the walker can move to the right or left in each step on a line. Since the complex phase of the coin operator C does not affect the probability distribution as discussed in [26], here we consider a constant coin with the parameter $\rho \in [0, 1]$,

$$C(\rho) = \begin{pmatrix} \sqrt{\rho} & \sqrt{1-\rho} \\ \sqrt{1-\rho} & -\sqrt{\rho} \end{pmatrix}. \quad (2)$$

To examine the recurrence characteristics of the two schemes, it is necessary to employ distinct evolution operators for characterizing the measurement procedure and, consequently, deriving the recurrence probabilities.

A. Unmonitored and monitored recurrence of QWs

Without loss of generality, we define the initial state of the QW system as $|\Psi(0)\rangle$ located at the origin. In the UMM scheme, the evolution of the unmonitored QWs is described

by the unitary evolution operator U . The state of the walker after t steps (t is an integer) is given by $|\Psi(t)\rangle = U^t|\Psi(0)\rangle$. The return of the walker to the origin, referred to as site recurrence, can also be interpreted as a subspace recurrence [27]. Here we focus only on the probability sense of the walker returning to the origin after t steps,

$$p(0, t) = \|\langle 0|U^t\Psi(0)\rangle\|^2, \quad (3)$$

and are not interested in the coin state.

For the MM scheme, after the first step, an absorbing sink [28] is placed at the origin to monitor the walker. The sink is modeled by a projection operator $\Pi_0 = |0\rangle\langle 0|$, which sets the amplitude at the origin to zero. The evolution of the monitored QWs is given by the nonunitary evolution operator

$$\tilde{U} = (I - \Pi_0)U. \quad (4)$$

Suppose the walker has survived the first $t - 1$ steps; then the first return probability at the origin until t steps is obtained from

$$q(0, t) = \|\langle 0|U\tilde{U}^{t-1}\Psi(0)\rangle\|^2. \quad (5)$$

For more details about the above derivation process of $p(0, t)$ and $q(0, t)$, refer to Appendix A.

Two inequivalent definitions for recurrence due to the non-trivial impact of measurements on the wave function of the quantum walker exist. To minimize measurement disturbance, Štefaňák *et al.* proposed one definition for the recurrence probability in QWs:

$$\mathcal{P}^{\text{UMM}} = 1 - \prod_{t=1}^{+\infty} [1 - p(0, t)]. \quad (6)$$

According to this definition, the UMM scheme involves the free evolution of a walker for a certain number of steps, followed by a single measurement at the origin after t steps, and then the walk is restarted. The results indicate that the recurrence properties of QWs are determined by the asymptotic behavior of the probability at the origin $p(0, t)$. The infinite product $\prod_{t=1}^{+\infty} [1 - p(0, t)]$ vanishes if and only if the series $\sum_{t=1}^{+\infty} p(0, t)$ diverges, and then $\mathcal{P}^{\text{UMM}} = 1$; otherwise, the infinite product does not vanish, and $\mathcal{P}^{\text{UMM}} < 1$.

Grünbaum *et al.* [21] proposed an alternative definition for the recurrence probability of QWs similar to the Pólya definition for the recurrence of RWs:

$$\mathcal{P}^{\text{MM}} = \sum_{t=1}^{+\infty} q(0, t). \quad (7)$$

This definition considers the MM scheme, which requires one to monitor the origin after each step and in which the walk ends if the walker is found. In the classical case, the two definitions are equivalent in the sense that $\mathcal{P}^{\text{UMM}} = 1$ if and only if $\mathcal{P}^{\text{MM}} = 1$ and vice versa. This arises from the fact that there is a relation between the first return probability $q(0, t)$ and the probability at the origin $p(0, t)$ in the classical case. Considering the nature of quantum measurements, however, the equivalence between these probabilities no longer holds in the quantum case. For example, the recurrence probability of Hadamard walks on a line is $\mathcal{P}^{\text{UMM}} = 1$, while $\mathcal{P}^{\text{MM}} < 1$.

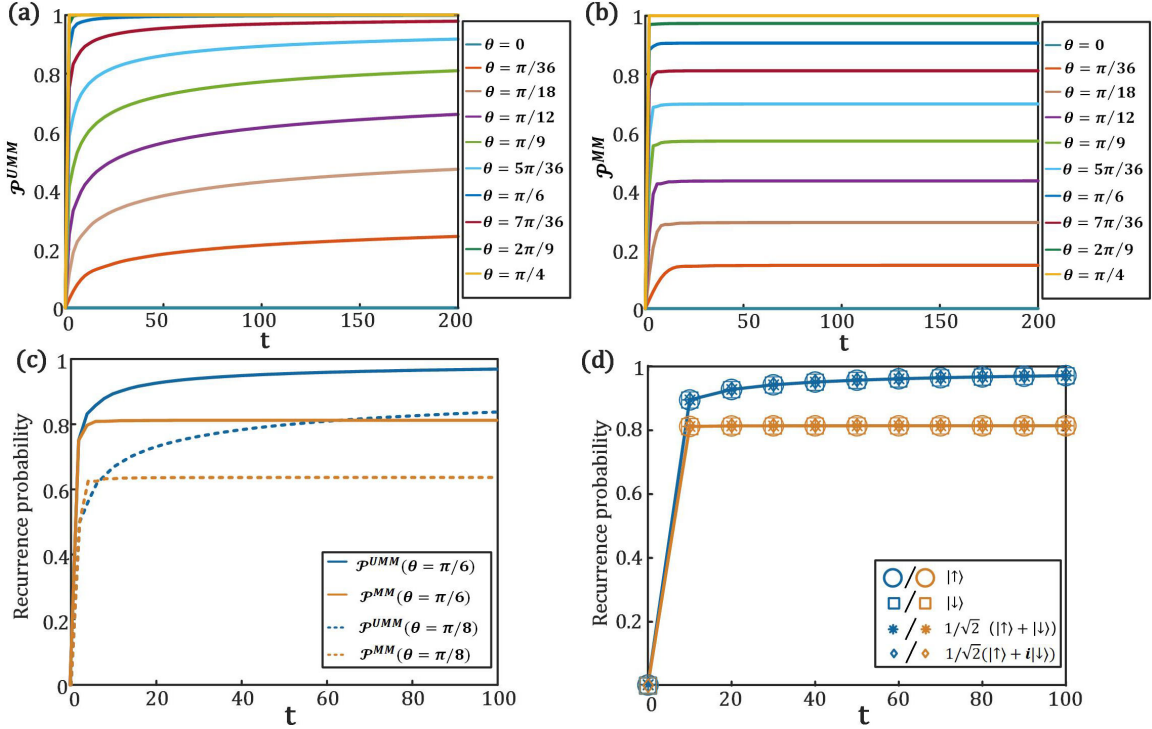


FIG. 1. The numerical simulation results. (a) The recurrence probability \mathcal{P}^{UMM} as a function of the steps t for different coin parameters in the UMM scheme. (b) The recurrence probability \mathcal{P}^{MM} as a function of the steps t for different coin parameters in the MM scheme. (c) The recurrence probabilities of two schemes varying with the steps t under different coin parameters $\theta = \pi/6$ and $\theta = \pi/8$. (d) The recurrence probabilities of both schemes with different initial coin states. The coin parameter is chosen to be $\theta = \pi/6$; blue and orange represent the UMM and MM schemes, respectively.

B. Influence of coin parameters on the recurrence probability

An unbiased QW on a line, also known as a Hadamard walk, exhibits properties such as unbiased coins and equal step lengths. The recurrent nature of this phenomenon is evident in both schemes. Additionally, we also note a class of biased QWs on a line characterized by biased coins and unequal step lengths. Consider the biased QWs on a line, where the coin parameter is denoted as ρ and the walker can move to the right (with a step length of 1) or the left (with a step length of r) in each step. A relationship between the coin parameter ρ and the length of the step r in the unmonitored recurrence of QWs [20] exists:

$$\rho(r) = \left(\frac{r-1}{r+1} \right)^2. \quad (8)$$

This equation provides the condition for the biased QWs on a line to exhibit recurrence: e.g., for $\rho \geq \rho(r)$, the QWs is recurrent; otherwise, $\rho < \rho(r)$, and the QWs is transient. A particular example involves equal step lengths when moving to the left or to the right; i.e., if $r = 1$, then $\rho(1) = 0$. Since the coin parameter satisfies the condition $0 \leq \rho \leq 1$, then $\rho \geq \rho(1)$ always exist. This means that an unmonitored QW on a line with equal step lengths is always recurrent ($\mathcal{P}^{UMM} = 1$), independent of the choice of the coin parameter. However, the value of the coin parameter ρ significantly influences the decay of the infinite product, thereby affecting the rate at which \mathcal{P}^{UMM} converges to its asymptotic limit. Therefore, it

is necessary to analyze the effect of different coin parameters on the convergence of the recurrence probability \mathcal{P}^{UMM} .

As an example, we simulate the curve of the recurrence probability \mathcal{P}^{UMM} as a function of the steps t for various values of θ (where $\rho = \cos^2(2\theta)$, $\theta \in [0, \pi/4]$). As shown in Fig. 1(a), with the same number of steps t , the convergence to an asymptotic limit of the recurrence probability is notably rapid as θ increases. Hence, it is possible to manipulate the value of the recurrence probability \mathcal{P}^{UMM} for unmonitored QWs on a line with equal step lengths by altering the coin parameter. Note that when $\theta = 0$, the recurrence probability constantly remains zero for all steps t , indicating that the walker will never return to the origin. Furthermore, the recurrence probability value for monitored QWs on a line with equal step lengths is also influenced by the coin parameter. The correlation between the coin parameter ρ and the recurrence probability \mathcal{P}^{MM} is given by [21,23]

$$\mathcal{P}^{MM} = 2 \frac{\sqrt{\rho} \sqrt{1-\rho} + (1-2\rho) \arccos(\sqrt{\rho})}{\pi(1-\rho)}. \quad (9)$$

We also conduct simulations to analyze the curve of recurrence probability \mathcal{P}^{MM} as a function of steps t for different values of θ . As shown in Fig. 1(b), an increase in the value of θ corresponds to a higher limit value of the recurrence probability \mathcal{P}^{MM} . Moreover, the recurrence-probability convergence to the asymptotic limit is relatively fast as the value of θ increases. Specifically, when $\theta = 2\pi/9$, the limit value $\mathcal{P}^{MM} = 0.9735$, whereas when $\theta = \pi/36$, the limit value

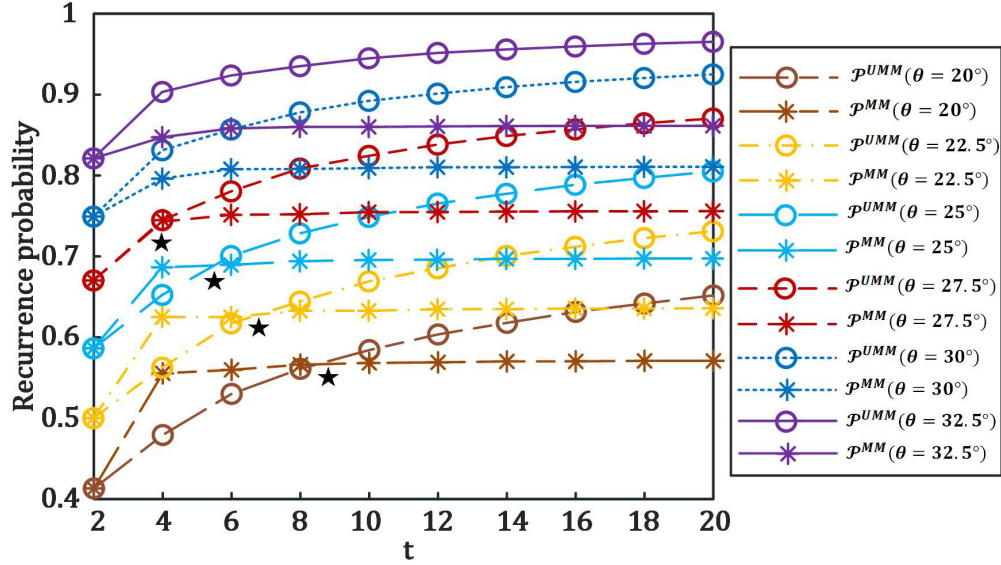


FIG. 2. The numerical simulation results. For different coin parameters θ , the recurrence probabilities (\mathcal{P}^{UMM} and \mathcal{P}^{MM}) of both schemes are a function of steps t . The black stars indicate the cases where the two recurrence probabilities are equal.

reduces to $\mathcal{P}^{\text{MM}} = 0.1478$, and these limit values comply with Eq. (9).

Therefore, the dependence of unmonitored and monitored QWs with equal step lengths on a line on the coin parameter opens up the possibility to design the value of recurrence probabilities. As an example, we conduct numerical simulations to illustrate the curves of the two recurrence probabilities as a function of steps t for different coin parameters $\theta = \pi/6$ and $\theta = \pi/8$ simultaneously. As shown in Fig. 1(c), the simulation results indicate that for both schemes, larger recurrence probabilities and faster convergence are achieved when using coin parameter $\theta = \pi/6$. In particular, for the UMM scheme, $\mathcal{P}_{t=100}^{\text{UMM}}(\theta = \pi/8) = 0.8376$, while $\mathcal{P}_{t=100}^{\text{UMM}}(\theta = \pi/6) = 0.9691$. The distance $|0.8376 - 1| > |0.9691 - 1|$; then when $\theta = \pi/6$, the recurrence probability \mathcal{P}^{UMM} converges to limit value at a faster rate. For the MM scheme, the limit value $\mathcal{P}^{\text{MM}}(\theta = \pi/8) = 2/\pi$, while $\mathcal{P}^{\text{MM}}(\theta = \pi/6) = 0.8120$. And at $t = 64$, $\mathcal{P}^{\text{MM}}(\theta = \pi/6)$ converges to its limit value 0.8120, while $\mathcal{P}^{\text{MM}}(\theta = \pi/8)$ requires until $t = 68$ to converge to its limit value $2/\pi$. The value of $\theta = \pi/8$ corresponds to the well-known case of Hadamard walks. It is noteworthy that for both unmonitored and monitored QWs on a line, the two recurrence probabilities depend solely on the coin parameter and are independent of the initial coin state. By selecting $\theta = \pi/6$, we simulate the influence of different initial coin states $\{|\uparrow\rangle, |\downarrow\rangle, 1/\sqrt{2}(|\uparrow\rangle + |\downarrow\rangle), 1/\sqrt{2}(|\uparrow\rangle - i|\downarrow\rangle)\}$ on the recurrence probabilities of both schemes, as shown in Fig. 1(d). The results demonstrate that the values of recurrence probabilities remain unchanged with varying initial coin states, consistent with the previous findings of Refs. [21,23].

Considering the two definitions of the recurrence probability [Eqs. (6) and (7)], it is easy to see that the two recurrence probabilities \mathcal{P}^{UMM} and \mathcal{P}^{MM} are always equal for $t = 2$. No matter how the coin parameters θ are chosen, this equivalence relation is not affected. However, as the number of walk steps increases, the value of the coin parameter affects the

difference between \mathcal{P}^{UMM} and \mathcal{P}^{MM} . As shown in Fig. 2, we focus only on the variation of the two recurrence probabilities within 20 steps where $\theta \in [20^\circ, 32.5^\circ]$. Note that both cases $\theta = 30^\circ$ and $\theta = 32.5^\circ$ show a clear difference between \mathcal{P}^{UMM} and \mathcal{P}^{MM} from $t = 4$. Nevertheless, when $\theta \in [20^\circ, 27.5^\circ]$, except for $t = 2$, \mathcal{P}^{UMM} and \mathcal{P}^{MM} will be equal at larger t steps (see the black stars in Fig. 2). In particular, the case where $\mathcal{P}^{\text{UMM}} \simeq \mathcal{P}^{\text{MM}}$ occurs as early as at $t = 4$ for $\theta = 27.5^\circ$. That is, for $\theta \leq 27.5^\circ$, the difference between \mathcal{P}^{UMM} and \mathcal{P}^{MM} is only gradually observed from at least six steps ($t \geq 6$), while for $\theta > 27.5^\circ$, the difference is clearly observed from $t = 4$. Therefore, in order to experimentally show the difference in these two recurrence probabilities within a finite number of steps, we choose the coin parameter $\theta = 30^\circ$ for experimental demonstration.

C. Experimental implementation

To illustrate the recurrence behaviors of unmonitored and monitored QWs with a biased coin (where $\theta = 30^\circ$) on a line, we implement a quantum-walk setup based on the bulk-optics framework. Additionally, we utilize the heralded single-photon source to showcase distinct single-particle quantum dynamics in the two measurement schemes.

First, we consider the heralded single-photon source utilized in our experiment. As depicted in Fig. 3(a), a 405-nm continuous-wave diode laser with a power of 20 mW is employed to pump a 30-mm-long periodically poled potassium titanyl phosphate (PPKTP) crystal, resulting in the generation of photon pairs with a central wavelength of 810 nm. These photon pairs are produced through the type-II spontaneous parametric down-conversion process, where the signal and idler photons exhibit orthogonal polarizations. A half-wave plate and a polarizing beam splitter (PBS1) are utilized in tandem to modulate the output power. Two lenses are employed before and after the PPKTP crystal for beam focusing and collimation. Subsequently, the pumped laser is filtered

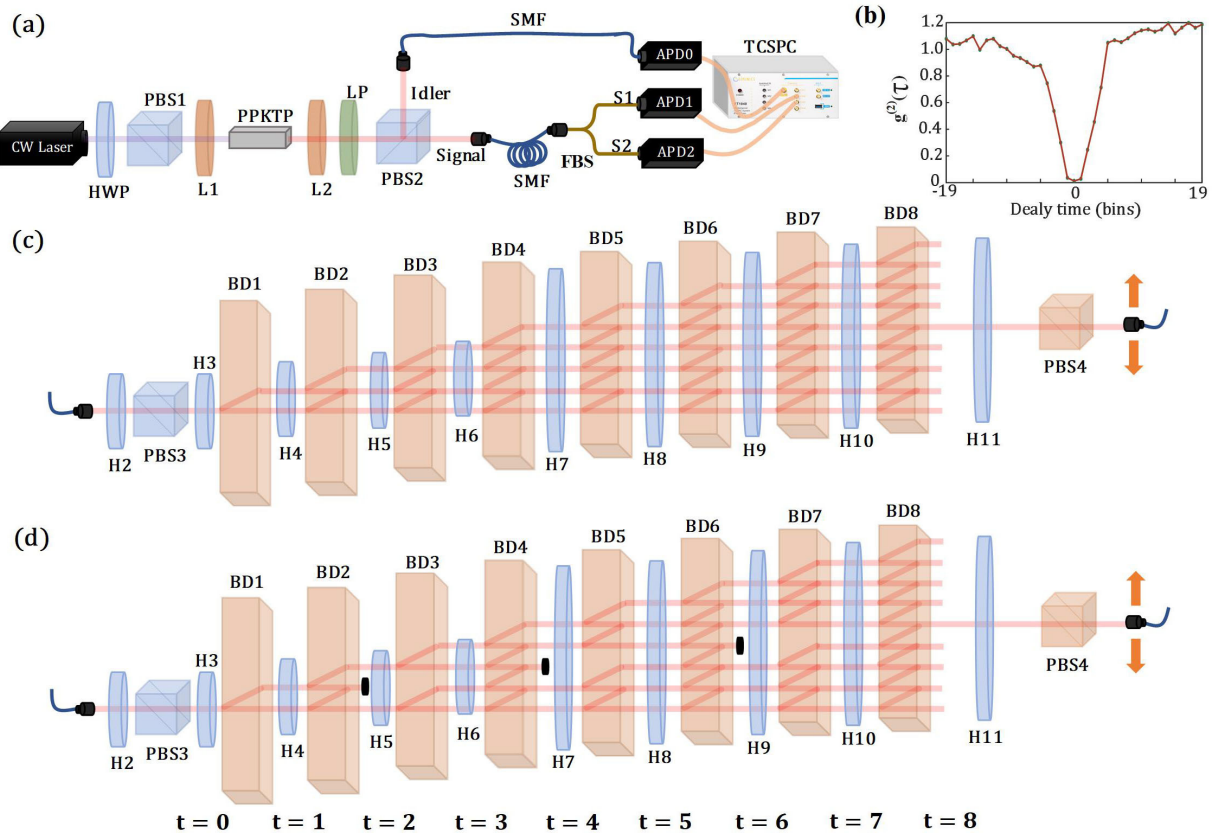


FIG. 3. Experimental setup for realizing the UMM and MM schemes using the QW system on a line. (a) The heralded single-photon source is prepared by spontaneous parameter down-conversion of a PPKTP crystal. (b) The second-order signal coherence function $g^{(2)}(\tau)$ is calculated under the condition of detecting an idler photon. (c) An unmonitored QW setup for implementing the UMM scheme. (d) The QW setup was monitored to implement the MM scheme, with the blocks representing the sinks placed at the origin position. In both QW setups, the initial state is prepared by signal photons passing through PBS3 and H3. At each step, a combination of H and BD is used to realize the coin operator and shift operation. The output signal photons are coupled into a SMF and subsequently detected using APD1, while the idler photons are detected by APD0. HWP and H: half-wave plate; PBS: polarizing beam splitters; L1 and L2: lenses; PPKTP: periodically poled potassium titanyl phosphate; LP: long-pass filter; FBS: fiber beam splitter; SMF: single-mode fiber; BD: beam displacer; APD: avalanche photon diode; TCSPC: time-correlated single-photon counting.

out using a long-pass filter, allowing for transmission of signal and idler photons which are then directed towards PBS2 for reflection or transmission, followed by coupling into two single-mode fibers (SMFs). One of the SMFs receiving idler photons is directly linked to an avalanche photon diode (APD0) with a dark-count rate of 100 s, while the other receiving signal photons is connected to a Hanbury Brown–Twiss (HBT) measurement setup. In the HBT interferometer, the signal photons are divided by a 50:50 fiber beam splitter into two arms (S1 and S2), which are then connected to APD1 and APD2 to measure the second-order correlation function $g^{(2)}(\tau)$ [29,30], where τ represents the time delay between APD1 and APD2. All APD clicks are recorded with 64-ps precision using a time-correlated single-photon counting (TCSPC) system. Consequently, the second-order correlation function $g^{(2)}(0) = 0.0119$ can be calculated for the single-photon light field of the signal following the APD0 trigger, and the result is shown in Fig. 3(b). It should be noted that the HBT setup in the signal-photon path appears only when measuring $g^{(2)}(\tau)$. In subsequent experiments, the signal-photon path will be connected to the QW setup through a SMF.

The signal photons are then routed into an eight-step QW setup comprising eight beam displacers (BDs) and several wave plates. In both unmonitored and monitored QW setups, the combination of half-wave plate 2 (H2) and PBS3 is utilized to control the number and polarization state of the input signal photons, as depicted in Figs. 3(c) and 3(d). The initial state of the QW system is represented by $\alpha|H, 0\rangle + \beta|V, 0\rangle$ ($|\alpha|^2 + |\beta|^2 = 1$), where the horizontal (vertical) polarization of photons indicates the coin state, and 0 signifies that the walker is initially at the origin. At each step, the coin operator C is executed by the half-wave plate set at 30° , while the shift operation S is performed by the BD. The BD's function is to allow $|V\rangle$ to pass through to $x - 1$ and $|H\rangle$ to be offset by 2.7 mm to $x + 1$. By executing eight combined operations of half-wave plates and BDs, an eight-step QW evolution can be achieved. Following this evolution, signal photons from the interferometric network are coupled into a measurement device consisting of H11 and PBS4, both of which are sufficiently large to permit nine beams of light to pass through simultaneously. The signal photons from all positions are sequentially detected by APD1 with a 2-ns time window. The coincidence signals, monitored via TCSPC, are

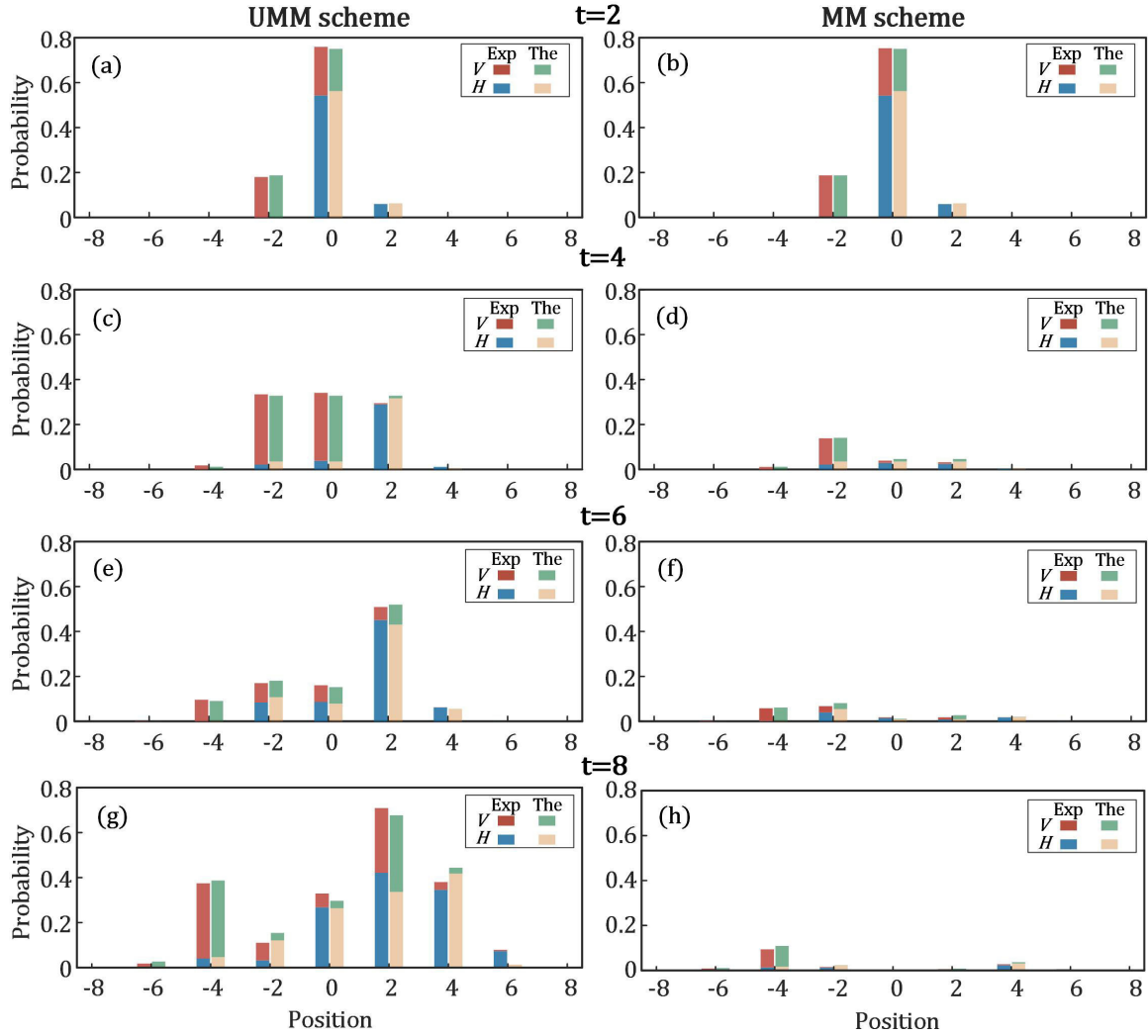


FIG. 4. Probability distributions of the walker over all positions of even steps for the UMM and MM schemes. The initial coin states of the unmonitored and monitored QW systems set here are $|H\rangle$. “The” and “Exp” represent the theoretical predictions and experimental results, and H and V represent the two measurement bases. Some bars of experimental values and theoretical predictions at positions -8 , -6 , 6 , and 8 are not shown due to the probability of the bars being less than 0.001 .

used to postselect single-photon events. Clicks are recorded for 1 s, resulting in a total of 1.1×10^5 coincidence counts.

In order to determine the recurrence probabilities, measurements are conducted at regular intervals in both schemes, specifically at even steps. Figure 3(c) illustrates the unmonitored QW setup utilized for the implementation of the UMM scheme. In the UMM scheme, measurements are conducted solely after even time steps without any intermediate operations. As depicted in Fig. 3(c), after two steps ($t = 2$), the measurement of all positions ($x = -2, 0, 2$) can be achieved by setting $H3 = H4 = 30^\circ$ and adjusting the action of the remaining wave plates and BDs to states that do not affect these photons. Subsequently, the photon counts at the three positions are successively recorded on the final detection port. The measurements of the remaining time steps can be implemented using similar procedures. Conversely, in the MM scheme, during the measurement at time step t , it is necessary to employ sinks for absorbing all photons at $x = 0$ in front of them, ensuring that the first arrival of the detected photons at $x = 0$ occurs precisely at time step t . The monitored QW setup

used to implement the MM scheme is shown in Fig. 3(d), where the sinks at the origin positions are represented by the blocks. For instance, when measuring at $t = 2$, there is no need to position absorption sinks upfront as there are no occurrences of $x = 0$. However, while measuring at $t = 4$, it becomes imperative to block the position $x = 0$ from $t = 2$; similarly, when measuring at $t = 6$, both positions $x = 0$ from $t = 2$ and $t = 4$ require blocking. Finally, when measuring at $t = 8$, all positions $x = 0$ from previous steps ($t = 2, 4, 6$) necessitate blocking. It should be noted that in both schemes, we built individual experimental setups for each even step to collect coincidence counts at all possible positions, which is necessary to obtain the probability distributions of photons.

The experimental results depicting the probability distributions of even steps for both schemes are illustrated in Fig. 4. In the two plots we show the conditional probability distributions of unmonitored and monitored QWs after eight steps with a biased coin ($\theta = 30^\circ$). It is evident that the walker has undergone distinct evolutionary processes in the two schemes. In particular, the initial coin state was chosen to be

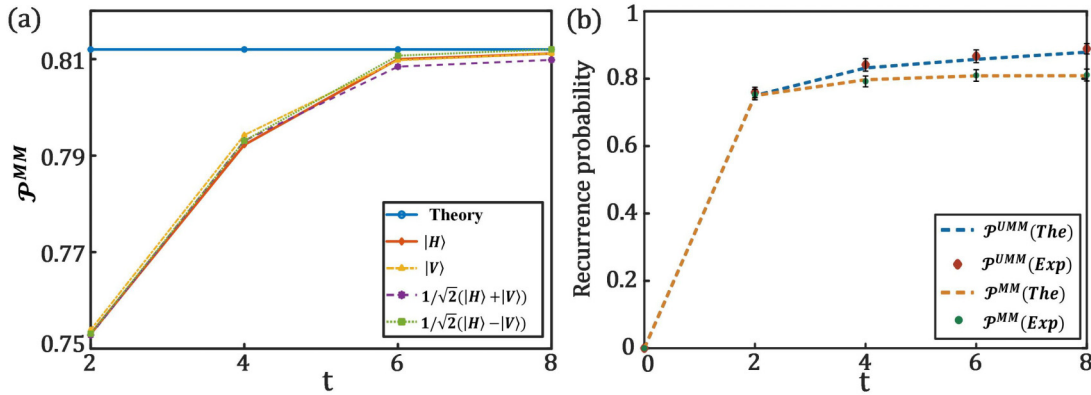


FIG. 5. Experimental results. (a) The recurrence probability \mathcal{P}^{MM} of different initial coin states in the MM scheme. At each step, the values of the data points are slightly different due to experimental errors. (b) The recurrence probabilities of the UMM and MM schemes of the eight-step QWs. The data dots denote the experimental results for recurrence probabilities in both schemes. The dashed lines represent the theoretical values expected from numerical simulations of the experiment. Error bars are derived from photon fluctuations and the accuracy of half-wave plates.

$|H\rangle \equiv (1, 0)^T$, resulting in an asymmetric conditional distribution in the MM scheme with absorbing sinks at the origin. In such a case the walker has a higher probability to be on the left side of the absorbing sink, as shown in Fig. 4. This result is different from the symmetric conditional probability distribution for Hadamard QWs simulated in Ref. [28], where the walker in the first step jumps to the left or to the right with equal probability. Alternatively, we consider the case with the impact of different initial coin states on the probability distribution in the MM scheme. The conditional probability distribution that results for different initial coin states of the monitored QWs can be found in Appendix B. Due to the choice of the initial coin state, the walker has a higher probability of being to the left or right of the absorbing sink, as well as a possibility of completely vanishing to either side of the absorbing sink. The selection of the initial coin state impacts the conditional probability distribution; however, the recurrence probability \mathcal{P}^{MM} of the MM scheme remains independent of the initial coin state. As shown in Fig. 5(a), the initial coin states were $\{|H\rangle, |V\rangle, 1/\sqrt{2}(|H\rangle + |V\rangle), 1/\sqrt{2}(|H\rangle - |V\rangle)\}$. Figure 5(a) shows that different initial coin states result in almost the same recurrence probability. Moreover, as the number of steps increases, the recurrence probability converges towards its theoretical value of 0.8120, which is derived from Eq. (9).

In addition, to quantitatively show the different evolution processes of the walker in the two schemes, we illustrate this feature in Appendix C for the case of the probability distribution over all positions. In the UMM scheme without sinks, measurements are conducted solely after even steps, resulting in an overall unitary evolution. Conversely, in the MM scheme, absorbing sinks are introduced at the origin following the first step and are modeled using a projection operator that nullifies the amplitude at the origin. Consequently, the overall evolution becomes nonunitary. Last but not least, we calculate the recurrence probabilities \mathcal{P}^{UMM} and \mathcal{P}^{MM} for both schemes using the resulting probability distributions mentioned above [refer to Appendix D for detailed information on the calculation of $p(0, t)$ and $q(0, t)$]. As expected, the two measurement schemes lead to different recurrence probabilities, and the

experimental results are shown in Fig. 5(b). The biased coin is used in order to reveal the difference between the two recurrence probabilities in fewer steps, and the difference between the two schemes can be clearly seen with four steps. Theoretically, as t increases, the recurrence probability \mathcal{P}^{UMM} of the UMM scheme converges to its limit value of 1, while the recurrence probability \mathcal{P}^{MM} of the MM scheme converges to its limit value of 0.8120. We conducted a proof-of-principle experiment with $t = 8$ solely for the purpose of illustrating the disparity in their recurrence behavior. It appears that the recurrence patterns of the two schemes exhibit significant difference from $t = 4$, and the empirical findings align with the theoretical projections.

III. DISCUSSION AND CONCLUSION

The probability that the walker returns to the origin during the time evolution is called the Pólya number of the walk. For balanced RWs, the Pólya number is uniquely determined by its dimensionality. Specifically, when $d = 1$ and $d = 2$, the Pólya number equals 1; for $d \geq 3$, it equals 0.3405. Because the walk space of a man is two-dimensional at most and a bird's walk space can be three-dimensional, we have the saying “a drunk man will find his way home, but a drunk bird may be lost forever.”

In this paper, we investigated the recurrence properties of QWs on a line using a biased coin for the UMM and MM schemes. Utilizing the bulk-optics framework for QWs with a single-photon source, we demonstrated the distinction between unitary evolution without sinks and nonunitary evolution with sinks in both schemes within eight-step QWs. Most significantly, we analyzed the influence of the coin parameter on the recurrence probability for unmonitored and monitored QWs on a line. QWs serve as a valuable tool that can be easily integrated into linear optical systems, allowing for implementation within various optical frameworks. While the two schemes for recurrence have been implemented in a time-multiplexing quantum-walk experiment with coherent light, single-photon QWs with bulk optical elements as an alternative tool have no relevant experimental validation. Here

we successfully implemented QWs using bulk optics and discussed the different recurrence behaviors of QWs in different measurement schemes. Our research not only expands the practical applications of QWs but also offers a valuable approach for investigating measurement-induced recurrence. Specifically, our focus is on analyzing the site-recurrence probability of a two-state quantum walk on a line, where the walker can move right or left with equal step lengths in each iteration. The implementation of the shift operator in our quantum-walk setup with bulk optics allows for easy manipulation based on positions. Looking ahead, we aim to further explore the recurrence properties of two-state quantum walks on a line with unequal step lengths.

ACKNOWLEDGMENTS

We are grateful to Dr. J. Li for participating in a theoretical discussion of this work. This work was supported by the National Nature Science Foundation of China (NSFC; Grant No. 92365115).

APPENDIX A: EVOLUTION OF UNMONITORED AND MONITORED QWs

We write the initial state of the QW system as

$$|\Psi(0)\rangle = (\alpha|\uparrow\rangle + \beta|\downarrow\rangle) \otimes |x\rangle, \quad (\text{A1})$$

where $|\alpha|^2 + |\beta|^2 = 1$. The evolution of the unmonitored QWs is given by the unitary evolution operator U , where the measurement at the origin is performed only once after t steps. Then the state of the walker after t steps is given by U in the initial state,

$$|\Psi(t)\rangle = U^t |\Psi(0)\rangle. \quad (\text{A2})$$

The probability distribution to find the walker at position x after t steps generated by the unmonitored QWs is written as

$$p(x, t) = \|\langle x|U^t \Psi(0)\rangle\|^2. \quad (\text{A3})$$

So the probability that the walker returns to the origin $x = 0$ at t steps is given by

$$p(0, t) = \|\langle 0|U^t \Psi(0)\rangle\|^2. \quad (\text{A4})$$

A quantum walk with the sink at the origin corresponds to the MM scheme for recurrence, in which the return to the origin is marked by the absorption of the walker. If the walker returns to the origin, it is absorbed by the sink, and the walk ends. The sink is modeled by a projection operator which sets the amplitude at the origin to zero while the states at the remaining positions are unchanged. Mathematically, the sink is described by the projection operator $I - \Pi_0 = I - |0\rangle\langle 0|$, which acts on the position state $|x\rangle$ as

$$(I - \Pi_0)|x\rangle = \begin{cases} 0 & \text{if } x = 0, \\ |x\rangle & \text{if } x \neq 0. \end{cases} \quad (\text{A5})$$

The evolution of a QW with the absorbing sink at the origin is described by alternating the projection operator $I - \Pi_0$ with the unitary operator U before the walker is detected, that is, $\tilde{U} = (I - \Pi_0)U$. Suppose that the walker is not detected at the origin until t steps, that is, it has survived the action of

sinks in the previous $t - 1$ steps; then the state of the walker after t steps is given by

$$\begin{aligned} |\Psi(t)\rangle_{\text{sur}} &= U|\Psi(t-1)\rangle \\ &= \frac{1}{\sqrt{s_{t-1}}} U \tilde{U}^{t-1} |\Psi(0)\rangle, \end{aligned} \quad (\text{A6})$$

where s_{t-1} is the normalized coefficient, also called the survival probability, and it is denoted by

$$s_{t-1} = \|\tilde{U}^{t-1} |\Psi(0)\rangle\|^2. \quad (\text{A7})$$

Using $|\Psi(t)\rangle_{\text{sur}}$, one can determine the probability that the walker is detected at the origin $x = 0$ after t steps:

$$\begin{aligned} p(0, t)_{\text{sur}} &= \|\langle 0|\Psi(t)_{\text{sur}}\rangle\|^2 \\ &= \frac{1}{s_{t-1}} \|\langle 0|U \tilde{U}^{t-1} |\Psi(0)\rangle\|^2. \end{aligned} \quad (\text{A8})$$

Then the first return probability of the walker until t steps is obtained from

$$\begin{aligned} q(0, t) &= s_{t-1} p(0, t)_{\text{sur}} \\ &= \|\langle 0|U \tilde{U}^{t-1} |\Psi(0)\rangle\|^2. \end{aligned} \quad (\text{A9})$$

APPENDIX B: CONDITIONAL PROBABILITY DISTRIBUTIONS FOR DIFFERENT INITIAL COIN STATES OF THE MONITORED QWs

In this Appendix, we present experimental results for the conditional probability distribution of the monitored QWs with an absorbing sink positioned at the origin for various initial coin states. In this example, we examine the identical coin operations that act on both the origin and the positive or negative half-line. Thus, the evolutions of the walker on both the origin and the positive or negative half-line are determined by

$$C(\theta = 30^\circ) = \frac{1}{2} \begin{pmatrix} 1 & \sqrt{3} \\ \sqrt{3} & -1 \end{pmatrix}. \quad (\text{B1})$$

The initial coin states were chosen to be $\{|H\rangle, |V\rangle, 1/\sqrt{2}(|H\rangle + |V\rangle), 1/\sqrt{2}(|H\rangle - |V\rangle)\}$, which result in different conditional probability distributions. Since the coin parameters remain constant, the walker exhibits identical diffusion speeds on both the positive and negative half-lines. For instance, after eight steps, the walker will arrive at nine positions: $-8, -6, -4, -2, 0, 2, 4, 6$, and 8 . Due to the selection of initial coin states $|H\rangle \equiv (1, 0)^T$ and $1/\sqrt{2}(|H\rangle - |V\rangle) \equiv 1/\sqrt{2}(1, -1)^T$, the conditional probability distribution exhibits a bias towards the negative half-line (i.e., the left side of the absorbing sink), as illustrated in Figs. 6(a1)–6(a4) and 6(d1)–6(d4). Similarly, as a result of selecting the initial coin states $|V\rangle \equiv (0, 1)^T$ and $1/\sqrt{2}(|H\rangle + |V\rangle) \equiv 1/\sqrt{2}(1, 1)^T$, the conditional probability distributions demonstrate a bias towards the positive half-line, as shown in Figs. 6(b1)–6(b4) and 6(c1)–6(c4). Furthermore, when the polarization state is not taken into account, the probability distributions of $|H\rangle$ and $|V\rangle$ and $1/\sqrt{2}(|H\rangle + |V\rangle)$ and $1/\sqrt{2}(|H\rangle - |V\rangle)$ exhibit symmetric relationships, respectively. The experimental results demonstrate that the selection of the initial coin state significantly impacts the

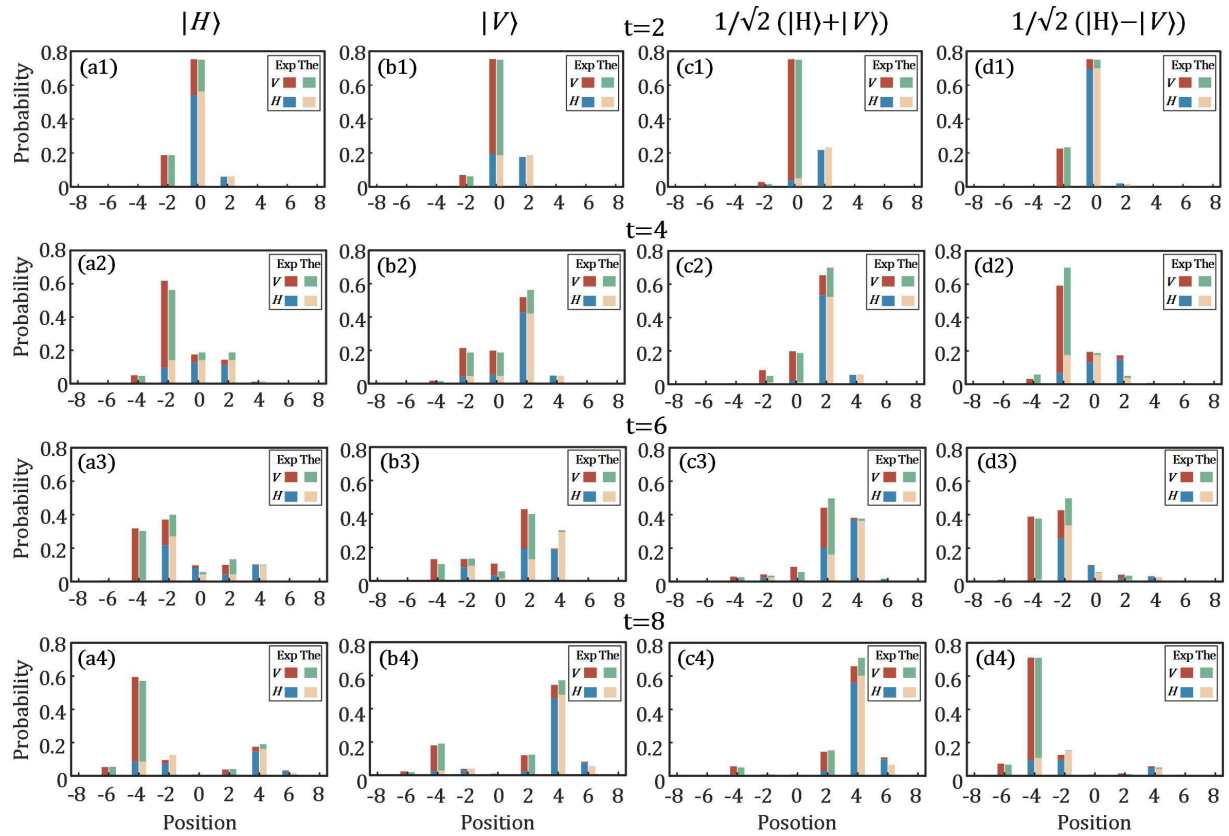


FIG. 6. Conditional probability distribution of the monitored QWs with an absorbing sink at the origin. The different initial coin states were chosen as $\{|H\rangle, |V\rangle, 1/\sqrt{2}(|H\rangle + |V\rangle), 1/\sqrt{2}(|H\rangle - |V\rangle)\}$. The biased coin has $\theta = 30^\circ$. Some bars of experimental values and theoretical predictions at positions $-8, -6, 6,$ and 8 are not shown due to the probability of the bars being less than 0.001 .

conditional probability distribution such that the walker has a higher probability of being to the left or right of the absorbing sink.

Additionally, we take into account the case in which the walker transitions to one side of the line with a probability of 1 during the first step based on the relationship between the initial coin state and coin operation $C(\theta = 30^\circ)$. Through theoretical analysis, we find that when the initial coin state is chosen to be $1/2(1, \sqrt{3})^T$, the walker can be found only on the positive half-line. However, when the initial coin state is $1/2(\sqrt{3}, -1)^T$, the walker will only be present in the negative half-line.

APPENDIX C: PROBABILITY DISTRIBUTIONS OVER ALL POSITIONS OF THE UNMONITORED AND MONITORED QWs

In this Appendix, we quantitatively compare the different evolution processes of the walker in the two schemes by showing the probability distributions of all time steps. The initial coin state was chosen to be $|H\rangle$, and the coin operator at each step is $C(\theta = 30^\circ)$. The probability distribution of the walker across all positions is depicted for both the UMM and MM schemes, as illustrated in Fig. 7. In the UMM scheme, we examine the evolution of unmonitored QWs without sinks,

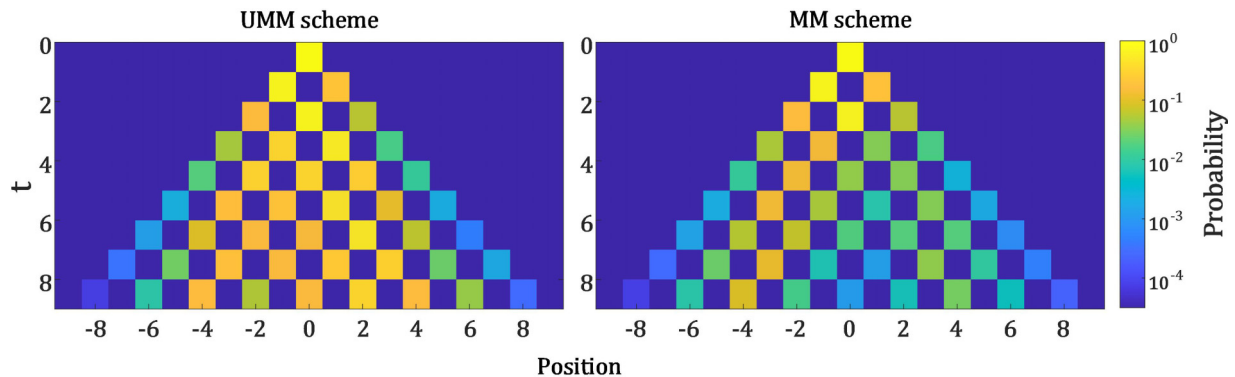


FIG. 7. The probability distribution over all positions of the UMM scheme without sinks and the MM scheme with sinks. Different colors are used to indicate the number of photons at each position.

which is characterized by the unitary evolution operator U . Conversely, in the MM scheme, we investigate the evolution of monitored QWs with sinks, described by the nonunitary evolution operator \tilde{U} . The absorption sinks located at the origin are evident in a region with low photon numbers around $x = 0$ in the MM scheme.

APPENDIX D: COINCIDENCE COUNTS AND PROBABILITIES IN BOTH SCHEMES

In this Appendix, we provide the method for determining the probability $p(0, t)$ in the UMM scheme and the probability $q(0, t)$ in the MM scheme through coincidence counts of photons. For the UMM scheme, we measure the coincidence counts $C(x, t)$ at all possible positions, and $p(0, t)$ is given by

$$p(0, t) = \frac{C(0, t)}{\sum_x C(x, t)}, \quad (\text{D1})$$

where $C(0, t)$ is the coincidence counts for position $x = 0$ at step t and $\sum_x C(x, t)$ is the total coincidence counts for all position at step t .

In the MM scheme, the sinks at $x = 0$ are achieved by absorbing all photons at these positions, resulting in a projection measurement onto the subspace of nonzero positions. As depicted in Fig. 3(d) in the main text, during measurements at step t ($t = 2, 4, 6, 8$), black blocks should be utilized to absorb all photons at $x = 0$ ahead of it to ensure that the

photon detected at step t reaches $x = 0$ for the first time. To investigate recurrence in the MM scheme, it is essential to determine the probability $q(0, t)$ of the first return to the origin. Like for the UMM scheme, we record coincidence counts $C(x, t)_{\text{sur}}$ at all possible positions at step t . The probability $p(0, t)_{\text{sur}}$ is written as

$$p(0, t)_{\text{sur}} = \frac{C(0, t)_{\text{sur}}}{\sum_x C(x, t)_{\text{sur}}}, \quad (\text{D2})$$

where $C(0, t)_{\text{sur}}$ is the surviving coincidence counts at position $x = 0$ until step t . $\sum_x C(x, t)_{\text{sur}}$ is the total coincidence counts in which the walker has not been absorbed during the first $t - 1$ steps and survives until step t . To get the first return probability $q(0, t)$ according to Eq. (19) of the main text, we need to calculate the product of the probability $p(0, t)_{\text{sur}}$ and the survival probability s_{t-1} that the walker was not absorbed at the origin during the first $t - 1$ steps and survives until step t ; the survival probability can be calculated as

$$s_{t-1} = \frac{\sum_x C(x, t)_{\text{sur}}}{\sum_x C(x, t)}. \quad (\text{D3})$$

Hence, the first return probability $q(0, t)$ can be expressed as

$$q(0, t) = \frac{C(0, t)_{\text{sur}}}{\sum_x C(x, t)}. \quad (\text{D4})$$

-
- [1] N. Güllotin-Plantard and R. Schott, *Dynamic Random Walks: Theory and Application* (Elsevier, Amsterdam, 2006).
- [2] G. Pólya, Über eine Aufgabe der Wahrscheinlichkeitsrechnung betreffend die Irrfahrt im Strabennetz, *Math. Ann.* **84**, 149 (1921).
- [3] B. D. Hughes, *Random Walks and Random Environments*, Vol. 1, *Random Walks* (Oxford University Press, Oxford, 1995).
- [4] Y. Aharonov, L. Davidovich, and N. Zagury, Quantum random walks, *Phys. Rev. A* **48**, 1687 (1993).
- [5] M. Genske, W. Alt, A. Steffen, A. H. Werner, R. F. Werner, D. Meschede, and A. Alberti, Electric quantum walks with individual atoms, *Phys. Rev. Lett.* **110**, 190601 (2013).
- [6] F. Zähringer, G. Kirchmair, R. Gerritsma, E. Solano, R. Blatt, and C. F. Roos, Realization of a quantum walk with one and two trapped ions, *Phys. Rev. Lett.* **104**, 100503 (2010).
- [7] C. A. Ryan, M. Laforest, J. C. Boileau, and R. Laflamme, Experimental implementation of a discrete-time quantum random walk on an NMR quantum-information processor, *Phys. Rev. A* **72**, 062317 (2005).
- [8] H. B. Perets, Y. Lahini, F. Pozzi, M. Sorel, R. Morandotti, and Y. Silberberg, Realization of quantum walks with negligible decoherence in waveguide lattices, *Phys. Rev. Lett.* **100**, 170506 (2008).
- [9] A. Peruzzo, M. Lobino, J. C. F. Matthews, N. Matsuda, A. Politi, K. Poulios, X. Q. Zhou, Y. Lahini, N. Ismail, K. Wörhoff, Y. Bromberg, Y. Silberberg, M. G. Thompson, and J. L. O'Brien, Quantum walks of correlated photons, *Science* **329**, 1500 (2010).
- [10] A. Schreiber, A. Gábris, P. P. Rohde, K. Laiho, M. Štefaňák, V. Potoček, C. Hamilton, I. Jex, and C. Silberhorn, A 2D quantum walk simulation of two-particle dynamics, *Science* **336**, 55 (2012).
- [11] K. Wang, X. Qiu, L. Xiao, X. Zhan, Z. Bian, W. Yi, and P. Xue, Simulating dynamic quantum phase transitions in photonic quantum walks, *Phys. Rev. Lett.* **122**, 020501 (2019).
- [12] S. Tornow, and K. Ziegler, Measurement-induced quantum walks on an IBM quantum computer, *Phys. Rev. Res.* **5**, 033089 (2023).
- [13] Y.-J. Wang, R.-Y. Yin, L.-Y. Dou, A.-N. Zhang, and X.-B. Song, Quantum first detection of a quantum walker on a perturbed ring, *Phys. Rev. Res.* **5**, 013202 (2023).
- [14] R. Yin, K. Ziegler, F. Thiel, and E. Barkai, Large fluctuations of the first detected quantum return time, *Phys. Rev. Res.* **1**, 033086 (2019).
- [15] F. Thiel, E. Barkai, and D. A. Kessler, First detected arrival of a quantum walker on an infinite line, *Phys. Rev. Lett.* **120**, 040502 (2018).
- [16] H. Friedman, D. A. Kessler, and E. Barkai, Quantum renewal equation for the first detection time of a quantum walk, *J. Phys. A* **50**, 04LT01 (2017).
- [17] H. Friedman, D. A. Kessler, and E. Barkai, Quantum walks: The first detected passage time problem, *Phys. Rev. E* **95**, 032141 (2017).
- [18] M. Štefaňák, I. Jex, and T. Kiss, Recurrence and Pólya number of quantum walks, *Phys. Rev. Lett.* **100**, 020501 (2008).
- [19] M. Štefaňák, T. Kiss, and I. Jex, Recurrence properties of unbiased coined quantum walks on infinite d -dimensional lattices, *Phys. Rev. A* **78**, 032306 (2008).
- [20] M. Štefaňák, T. Kiss, and I. Jex, Recurrence of biased quantum walks on a line, *New J. Phys.* **11**, 043027 (2009).

- [21] F. A. Grünbaum, L. Velázquez, A. H. Werner, and R. F. Werner, Recurrence for discrete time unitary evolutions, *Commun. Math. Phys.* **320**, 543 (2013).
- [22] T. Nitsche, S. Barkhofen, R. Kruse, L. Sansoni, M. M. Štefaňák, A. Gábris, V. Potoček, T. Kiss, I. Jex, and C. Silberhorn, Probing measurement-induced effects in quantum walks via recurrence, *Sci. Adv.* **4**, eaar6444 (2018).
- [23] M. M. Štefaňák, Monitored recurrence of a one-parameter family of three-state quantum walks, *Phys. Scr.* **98**, 064001 (2023).
- [24] A. Didi and E. Barkai, Measurement-induced quantum walks, *Phys. Rev. E* **105**, 054108 (2022).
- [25] S. Dhar, S. Dasgupta, A. Dhar, and D. Sen, Detection of a quantum particle on a lattice under repeated projective measurements, *Phys. Rev. A* **91**, 062115 (2015).
- [26] B. Tregenna, W. Flanagan, R. Maile, and V. Kendon, Controlling discrete quantum walks: Coins and initial states, *New J. Phys.* **5**, 83 (2003).
- [27] J. Bourgain, F. A. Grünbaum, L. Velázquez, and J. Wilkening, Quantum recurrence of a subspace and operator-valued Schur functions, *Commun. Math. Phys.* **329**, 1031 (2014).
- [28] M. Sabri, E. Segawa, and M. Štefaňák, Conditional limit measure of a one-dimensional quantum walk with an absorbing sink, *Phys. Rev. A* **98**, 012136 (2018).
- [29] E. Bocquillon, C. Couteau, M. Razavi, R. Laflamme, and G. Weihs, Coherence measures for heralded single-photon sources, *Phys. Rev. A* **79**, 035801 (2009).
- [30] D. Höckel, K. Lars, and B. Oliver, Direct measurement of heralded single-photon statistics from a parametric down-conversion source, *Phys. Rev. A* **83**, 013802 (2011).